M Spolaore et al.

H-mode Achievement and Edge Features in RFX-mod Tokamak Operation

H-mode Achievement and Edge Features in RFX-mod Tokamak Operation

M.Spolaore, R.Cavazzana, L.Marrelli, L.Carraro, P.Franz, S.Spagnolo, B.Zaniol, M.Zuin, L. Cordaro, S.Dal Bello, G. De Masi, A.Ferro, C.Finotti, L.Grando, P.Innocente, O.Kudlacek, G.Marchiori, E.Martines, B. Momo, R.Paccagnella, P.Piovesan,C.Piron, M.E.Puiatti, M.Recchia, P.Scarin, C.Taliercio, N. Vianello, L.Zanotto

Consorzio RFX, Padova, Italy

E-mail: `monica.spolaore@igi.cnr.it`

Abstract.
The RFX-mod experiment is a fusion device designed to operate as a Reversed Field Pinch (RFP), with a major radius R= 2 m and a minor radius a = 0.459 m. Its high versatility recently allowed operating also as an ohmic tokamak allowing comparative studies between the two configurations in the same device. The device is equipped with a state of the art MHD mode feedback control system, providing a magnetic boundary effective control, by applying resonant or non-resonant magnetic perturbations (MP) both in RFP and in tokamak configurations. In the fusion community the application of MPs is widely studied as a promising tool to limit the impact of plasma filaments and ELMs on plasma facing components. An important issue is envisaged in the exploitation of the RFX-mod active control system for ELM mitigation studies. As a first step in this direction, this paper will focus on the most recent achievements in term of RFX-mod tokamak explored scenarios, which allowed the first investigation of the ohmic and edge biasing induced H-mode. Among the others the realization of D-shaped tokamak discharges and the design and deployment of an insertable polarized electrode were accomplished. Reproducible H-mode phases were obtained with insertable electrode negative biasing stimulation in plasma shaped Single Null discharges, representing an unexplored scenario with this technique. Important modification of the edge plasma density and flow properties are observed. During the achieved H-mode ELM-like (Edge Localized Modes) electromagnetic composite filamentary structures are observed. They are characterized by clear vorticity pattern and parallel current.

30 March 2017

1. Introduction

Thanks to its high versatility RFX-mod experiment recently had been operated as an ohmic Tokamak, with a toroidal field up to 0.55T, extending the parameter range explored by other devices, for example in the very low $q(a) < 2$ region, and allowing comparative studies between circular cross-section tokamak and reversed field pinch configurations in the same device[1]. RFX-mod is equipped with a set of 192 actively controlled saddle coils arranged in 48 poloidal arrays, each of them consisting of 4 coils, fully covering the vessel torus. This system represents the state of the art of MHD mode feedback control [2]. It allows a noticeable flexibility, so that the magnetic boundary can be effectively controlled and modulated by applying resonant or non-resonant magnetic perturbations (MP) both in RFP and in tokamak configurations [3, 4]. RFX-mod is well suited to investigate the magnetic feedback control of the m=2, n=1 mode. The performed experiments have been fully successful for the stabilization of non-resonant RWM emerging in $q(a) < 2$ plasmas [2]. The device allowed also the development of advanced MHD instability control algorithms [5], contributing to the advancement of runaway electrons studies [6] and disruption mitigation techniques by magnetic feedback control. A further important issue is envisaged in the exploitation of the RFX-mod active control system for ELM mitigation studies, where the the application of MPs is widely studied as a promising tool to limit the impact of ELMs on plasma facing components [7]. As a first step in this direction, this paper will focus on the most recent achievements in term of tokamak discharge optimization, which allowed the first investigation of the ohmic and edge biasing induced H-mode in RFX-mod. In the last two years several developments have been performed to this end: in particular, the realization of D-shaped tokamak discharges (Single and Double Null) and the design and deployment of an insertable polarized electrode. The edge biasing technique was widely used in the past years [8] to induce confinement improvements in fusion experiments. In more recent experiments biasing was proposed for disruption avoidance due to the interaction of ExB flow with MHD modes [9, 10]. In the RFX-mod experiments reported in this paper, the edge biasing is applied on circular and on SN shaped discharges, the latter representing an unexplored scenario. The optimization of the plasma shaping allowed studying the interaction between the edge features associated to the two configurations and the externally induced current flowing through the plasma and the biased electrode.

The paper is organized as follows. The adopted experimental setup for electrode biasing operation and main diagnostic system involved are described in section 2. In Section 3 the experimental finding characterizing the achievement of H-mode regimes are described, including the comparison between the circular limited configuration and the Single Null (SN) configuration. Section 4 is devoted to the edge electromagnetic (EM) features observed during the H-mode, with special focus on one hand to the fine analysis of detected edge localized EM structures Section 4.1 and on the other, Section 4.2, hand to the investigation of the modes appearing on the edge magnetic fluctuations. Some conclusions are drawn in the last session Section 5.

2. Experimental setup and electrode operation

The RFX-mod experiment is a fusion device designed to operate as Reversed Field Pinch (RFP), with a major radius R= 2 m and minor radius a = 0.459 m, equipped with a first wall fully covered by graphite tiles. The development of reproducible and

controllable tokamak operation in this experiment tooks advantage of the implementation of a real-time feedback control of the electron density [11] and of the plasma shape. Shape control have been possible thanks to the flexibility of RFX-mod power supply and magnet system and to the design of a multi-variable shape feedback control system based on a full model based approach [12]. An algorithm to provide a fast and reliable plasma boundary reconstruction with a limited number of sensors has been developed and described in [13]. The algorithm accuracy has been benchmarked against simulation results provided by the Grad-Shafranov solver MAXFEA. Satisfactory reconstructions with differences below $8mm$ have been obtained. The algorithm also proved to be sufficiently robust against the noise observed in the experimental input signals. The evaluation of the time evolution of the plasma Last Closed Flux Surface (LCFS) shown in the following is performed with this method.

The electrode setup used for biasing experiment is show in the Figure 1. The electrode head consists of a graphite truncated ellipsoid ($115mm \times 25mm \times 65mm$). It is connected to a manipulator and inserted inside the plasma from an access located on the bottom part of the device, at the toroidal position $\phi = 262°30'$. The electrode head insertion inside the vacuum chamber is kept for the whole discharge duration. Depending on the plasma position and shape time evolution, the tip of the electrode has been inserted up to 8 cm inside the Last Closed Flux Surface (LCFS) during the experimental campaign.

The electrode head position with respect to the LCFS is schematically represented in top panels of Figure 2, where the corresponding poloidal section of the machine is represented. As an example the reconstructed shape and position of the LCFS, represented by the red line, is shown in the shot ♯39101, operated in circular configuration, and the shot ♯39135 in SN configuration. The time instants chosen for the two examples correspond to the phase of electrode biasing switched-on. For the shots shown in this paper the electrode insertion was ~ 7 cm inside the LCFS in both circular and SN plasma poloidal shaping.

The temperature of the electrode is monitored by an infrared camera in order to avoid its overheating. The temperature of the electrode surface has been measured by an infrared camera (Flir A655sc [14]), operating in the $7.5 \div 14\mu m$ infrared range with a time resolution up to 5 ms and an accuracy of $\pm 2°C$, installed in the external top port at the same poloidal section of the biasing electrode. In the bottom panels of Figure 2, the thermal map of the electrode probe head exposed to plasma on the two shots is shown, after the shot completion. The orientation of the electrode head is also shown with respect to the reference frame of the device. It is observed that the highest temperature values are achieved on the side at higher ϕ values. This observation confirms the expected higher temperature on the electrode side exposed to electron flux, given the (toroidal) plasma current $I_p > 0$.

Circular limited (CL) plasmas are operated with a 0.5-1 cm horizontal displacement towards the high field side, the inner first wall therefore acting as a toroidal limiter in this case. Features of performed circular discharges are plasma radius $r_{plasma} = 42 - 45cm$, $I_p = 60 - 95kA$, $q(a) = 2.7 - 4$, n_e up to $8 \cdot 10^{18}m^{-3}$. Single Null (SN) discharges are characterized by the X-point distance from the first wall $0.5 - 2cm$. SN discharges are somewhat smaller, $< r_{plasma} >= 36 - 39cm$, $I_p = 45 - 75kA$, $q_{95} = 2.5 - 4.5$, n_e up to $5 \cdot 10^{18}m^{-3}$.

The biasing circuit scheme is shown in Figure 3. The electrode has been feed using one of the main power supplies of the machine, a single quadrant 6-phases regulated

bridge [15]. An L-R network is used to filter the fire sequence of the thyristors (1.67 ms period) as shown in Figure 3. To preserve the electrode from damages, its power supply was controlled through the MARTe real-time control system of RFX-mod, programmed to turn off the power supply when the V-I curve was out of the expected range (i.e. arc occurrence). In the Figure 3 bottom panel, the explored range of voltage applied to the electrode V_{el} and the corresponding collected current,I_{el} is show. The data were collected during the electrode operation at different V_{el}. The reconstructed curve, obtained from a set of similar discharges in SN configuration in the whole experimental campaign, exhibits features typical of a Langmuir probe characteristic. In particular a tendency to saturation is observed towards negative V_{el} corresponding to a mainly ion current, $I_{el} < 0$, while much larger electron positive current are collected by positively biased electrode. As shown in Figure 3 both positive and negative voltage with respect to the vacuum chamber were explored, ranging from $-750V$ to $+350$, with I_{el} up to $\sim 300A$.

The positive voltage experiments did not provide noticeable effects on the edge properties during the performed campaign. It has to be noted however that the electron branch ($V_{el} > 0$) was limited in order to preserve the device, so that the collected data on positive electrode biasing are not exhaustive at this stage. A more extended campaign was performed on the other side with $V_{el} < 0$ operation, where transition to improved confinement plasma regimes were instead obtained with quite reproducible features[16].

The scope of this paper is to present the first results of biasing experiment in RFX-mod [17], focusing on the representative cases where the improved confinement fingerprint regimes is obtained.

The edge plasma parameter monitor presented in this paper is performed mainly with the insertable probe head called "U-probe" and spectroscopic diagnostics. The "U-probe" head, placed at $\phi = 247°30'$ consists in a probe head including 2D arrays of both electrostatic and magnetic sensors. The U-probe provides simultaneous measurements of quantities obtainable via different configuration of electrostatic sensors, such as radial profiles of plasma density, electron temperature, T_e, $E \times B$ flow and magnetic fluctuations, also the essential information for the identification and characterization of the EM filaments[18]: the direct measurements of current density and vorticity parallel to the edge main magnetic field. A picture of the U-probe insertable probe head is also shown in the insert of Figure 1, with the indication of the reference frame. The probe is inserted from the LFS at the equatorial plane.

RFX-mod features a multi-chord passive doppler spectroscopy diagnostic. Based on high resolution spectrometers and 2D CCD cameras, the diagnostic is capable to measure the poloidal and the toroidal flow of RFX main impurities, in particular carbon, oxygen and boron. The diagnostic time resolution may span from 1 to 20 ms, depending on the signal level of the impurity emissions, that are acquired along a selection of the 25 available lines of sight. In these particular experiments, C III toroidal flow velocity has been monitored. The strong emission of C III multiplet at 465 nm, allowed a time resolution of 5 ms, despite the low electron density of performed tokamak discharges. As for the radial position of the ion, whose Doppler temperature is of about 30 eV, transport simulation indicates a C III emission profile sharply peaked at about 0.9 normalised radius. For this reason we are confident that the measured impurity flow velocity is localised in the last 5 cm of the plasma edge, while the negative sign of the Doppler shift of the C III line emission indicates that the impurity flow has the same direction of the plasma current and the magnetic field.

Information on the core features are provided mainly from Soft X-Ray (SXR) radiation. SXR emission has been imaged by means of an advanced tomographic system [19], based on 100 lines of sights. The reconstruction technique is based on the truncated Fourier-Bessel expansion; the inversion of the resulting matrix equations is regularised by means of the Generalised Cross Validation technique (see [20] and the references contained therein).

3. H-mode achievement in RFX-mod tokamak operation

Indications of Ohmic H-mode were transiently observed on RFX-mod Single Null shaped plasmas, as attested by D_α drop and simultaneous increase of the SXR emission. These transient states seem to be related to fast plasma current ramp-down [21], work is in progress on this subject. The technique of edge biasing allowed, instead, to obtain more stable and reproducible H-mode phase, lasting for all the electrode operation. We will focus on the results obtained with negative voltage biasing with respect to the first wall. In this experimental condition circular and SN configurations will be compared.The negative electrode biasing induced in a quite reproducible way the H-mode achievement.Two representative shots were chosen, ♯39101 and ♯39135 respectively, operated in Deuterium.

An example of plasma features modifications induced by negative electrode biasing is shown in Figure 4 for the two representative discharges. In both shots the signature of a transition to improved confinement, H-mode, is observed. The achieved H-mode is characterized by similar behavior in the two configurations: an abrupt decrease of the D_α signals, measured along different lines of sight, an increase of the plasma electron density, n_e, though the puffing valve is switched off by the feedback system [11], the poloidal β_p, not shown in the picture, and the diamagnetic energy W_{dia} also increase. The spectroscopically determined edge toroidal flow becomes more negative in agreement with the $J_r \times B_\theta$ force, with the radial current density, J_r, directed inward. Important modifications can be inferred also in the edge radial profiles from the radial electric field, E_r, and the ion saturation current, I_{sat}, taken in this case as a proxy of the local time traces measured in the LCFS proximity by the insertable probe. In the following a more detailed analysis on the edge features will be shown. According to the performed experiments the conditions for the achievement of the transition to H-mode regime can be summarized as follows.

This occurs when V_{el} overcome a threshold value around 200-300V and for enough high average plasma density, $n_e = 1 - 3 \cdot 10^{18} m^{-3}$ for I_p= 70 - 80 kA. An experimental example of this finding is represented in Figure 5. In the left column are compared I_{el}, V_{el}, D_α, core plasma density n_e, in a case where the transition occurs (red line) and do not (black line). The sudden drop of the D_α is taken as signature of the occurred transition to improved regime. The two compared cases exhibit the same applied V_{el}, but a difference is observed in the plasma density and the transition occurs in the shot characterized by the higher density level. The right column of Figure 5 compares in a similar way two shots characterized by similar density levels before the transition. The two cases are characterized instead by a differently programmed V_{el}, and the transition is better related to the higher absolute value (red line) of applied voltage in the case where the transition is observed.

As a further piece of information the core behavior, as monitored by SXR radiation, was analyzed in the two representative cases of Figure 4. Core temperature data profiles are challenging at the low level of density characterizing these tokamak

discharges, however interesting information can be obtained from the SXR emissivity tomography reconstruction on poloidal section. Figure 6 shows the emissivity reconstruction for the limited circular and SN case reference examples, evaluated in a given instant preceding the electrode biasing phase. As in Figure 2 the red line in the poloidal sections indicates the evaluated position of the LCFS. A more symmetric emissivity is observed in the limited circular configuration. This aspect is well evidenced by the horizontal (along r) and vertical (along z) brightness (line integral) profiles shown on the respective right panels of Figure 2. The two brightness peaks are nearly overlapped in the circular configuration while a shift of about 20 cm is observed between the the horizontal and vertical brightness profiles in the SN case. The following Figure 7 is arranged with an analogous scheme, but the data are obtained during the established H-mode regime. Symmetry differences between the two emissivity shapes in the poloidal section are still visible, but during the H-mode phase a generalized increase of the brightness profile width is observed, indicating an increase of the plasma volume during the H-mode. In addition a noticeable increase, a factor 3 in the SN shape and up to a factor 10 in the circular shape, of the brightness peak is observed during the H-mode phase. This increase is clearly ascribable to the density increase for the example ♯39101, while impurities could also play a not negligible role in the ♯39135 case.

3.1. Edge profiles

In Figure 8 the $V_{el} - I_{el}$ characteristic during the biasing electrode operation in the shot ♯39101 is shown. The blue triangles indicate the H-mode phase, approximately from 710 to 990 ms, highlighted in Figure 4. It can be noted that the H-mode appears at $V_{el} > 250$V and for a given V_{el} the collected current I_{el} is lower during H-mode, corresponding to an increase of the plasma impedance during the H-mode. It has to be noted however that a dependence of the $V_{el} - I_{el}$ transition during the H-mode from the local plasma parameters as density and temperature is expected. The floating potential radial profile time evolution $V_f(r, t)$ is shown on the Figure 8 right side, the vertical dashed blue line indicates the electrode switching-on while the continuous lines delimitate the H-mode phase. The $V_f(r, t)$) profile measured by 5 pins radially covering 24 mm is clearly affected by the electrode action, but this effect is by far larger during the H-mode. This effect is clear and strong even accounting for the outer moving of the LCFS radial position, r_{LCFS}, (green line), then its approaching to the fixed U-probe radial location, provided by the magnetic reconstruction during this phase.

To disentangle this issue the radial profiles of different quantities, as measured by the U-probe, are reconstructed as a function of the relative distance between the measuring pin and the local position of the LCFS, $r_m = r - r_{LCFS}$. Representative results are shown in Figure 9 and Figure 10 for the two representative circular and SN discharges shown in Figure 4. The two towers of the U-probe are placed on the same poloidal section and are symmetrical with respect to the LFS equatorial plane. The profiles, as a function of r_m, of V_f, poloidal flow $v_{E \times B}$, ion saturation current, I_{sat}, and pressure $P_e = n_e T_e$, exploit data obtained from both towers. Looking at the circular limited shape Figure 9, the effect of the biasing induced transition to H-mode is clearly apparent from the $V_f(r_m)$ profiles. Different colors in the profiles (Figure 9 left column) refer to average values over 50 ms centered at different time instants, the blue one is the low confinement profile (L-mode) reference obtained

before the electrode operation. The same color code is used in the vertical lines during the time evolution of I_{el} and D_α (Figure 9 right column). During all the discharge the $V_f(r_m)$ stay around $V_f = 0$ (first wall potential) from $r_m > 1.5$ cm. Going towards the plasma center, profiles exhibit more negative values and about 4 times lower during the H-mode. This behavior reflects on the abrupt change in the poloidal $E \times B$ flow, calculated as $E_{r_m}/B_t \simeq dV_f(r_m)/dr_m/B_t$ where E_{r_m} is the radial electric field estimated in the approximation $dT_e(r_m) << dV_f(r_m)$. The poloidal $E \times B$ flow exhibits an increase of more than one order of magnitude in the region from $-0.5 > r_m > 1.5$ cm. The $v_{E \times B}$ shear layer expected in biasing experiments is then developed. Strong gradients are developed also in the $I_{sat}(r_m)$ and $P_e(r_m)$ in particular for in the $r_m < 0$ region. It can be observed that $\nabla_r P_e = 200 Pa/m$ during the L-mode increases up to $\nabla_r P_e = 700 Pa/m$ during the H-mode phase. In the right column of fig 4 is show also an interesting quantity represented by the shearing rate, $dv_{E \times B}/dr$, measured at r=0.422 m. A clear jump is observed during the electrode operation and in particular during the H-mode, reaching values around $5 \cdot 10^4/s$.

Even if the U-probe has the same radial insertion, r, for the two shots, in the SN shape, Figure 10, the region span across the LCFS is about double than the Figure 9. This is due to the poloidal asymmetry of configuration in the SN case (see Figure 2). This effect is apparent in the profiles of Figure 10, where a wider region is explored around r_{LCFS} and in particular in the $r_m < 0$ side. Vertical dashed lines in the Figure 9 and Figure 10 are inserted in the profiles plot as reference positions in the two cases. Coming then to the SN case the $V_f = 0$ position occurs about 1 cm outer with respect to the circular configuration, but the effect of H-mode inducing a steeper V_f profile is analogous. Noticeable values of poloidal $E \times B$ flow of the order of $10^4 m/s$ and shear, $10^5/s$ measured at r = 0.422m, are induced also in this case. The $I_{sat}(r_m)$ and $P_e(r_m)$ profiles exhibit as well strong gradients at the H-mode occurrence, reaching values inside LCFS $\nabla_r P_e = 150 Pa/m$ in the L-mode increasing up to $\nabla_r P_e = 450 Pa/m$ during the H-mode. It is found that the characteristic pressure length $L_{P_e} = |P_e/\nabla_r P_e| \sim 10^{-2}m$, double with respect to the circular case.

The H-mode phase is expected to reduce turbulence transport, so that in Figure 11 shows two quantities taken as representative of electrostatic and magnetic fluctuation behavior in the experiment under consideration. These are the parallel vorticity ω_t, calculated from the measurement of the U-probe pins arranged in a 2D array in the cross field plane, and the fluctuations of the radial component of the magnetic field, measured by one of the U-probe coils, δb_r. The ω_t spectrogram exhibits in both configurations a discontinuity in the H-mode phase, but while in the SN shot the higher frequency range is strongly depressed, the corresponding region in the circular case exhibits a mode at $f \sim 70$ kHz, together with those that appear its harmonics at higher frequencies. A similar feature is found on its magnetic counterpart but at frequencies larger than 100 kHz. On the other side the magnetic spectrogram for the SN case shows the presence of coherent modes during H-mode but at lower frequency. A more detailed analysis performed on these modes will be shown in Section 4.2.

4. Edge electromagnetic features during H-mode

A more detailed analysis of some phenomena observed in the phase when the transition to an improved confinement taking as a reference for this transition the fast drop of the D_α signal is proposed in this section. Specifically the focus will be devoted to the detailed analysis of localized structures emerging in this phase, Section 4.1, and to a

preliminary characterization of magnetic mode activity observed during the H-mode phase, Section 4.2.

4.1. Edge Localized EM structures during H-mode

During the electrode induced H-mode phase strong peaks, lasting about 1 ms, are detected sometimes on the D_α signal. These peaks occur with a repetition rate ranging from 50 to 400 Hz in the explored conditions. In the tokamak experiments this behavior is usually associated to the presence of Edge Localized Modes (ELM) [22], filamentary plasma structures, elongated along the magnetic field lines, characterized by a density higher than the surrounding plasma and ejected into the Scrape Off Layer region. The bursty behavior of the D_α monitor is related to the interaction of ELMs with the plasma wall or divertor plates. In general the presence of ELMs is observed during ohmic or additional heating assisted H-mode [23], while the biasing induced H-mode and in particular with a SN configuration is to our knowledge an unexplored experimental condition. A first observation from SXR measurements indicates that the revealed bursts are not correlated with the core sawtooth activity, suggesting an edge related behavior. In the examples of shot showed in the previous sections the presence of bursts is visible i.e. in the D_α signal of shot ♯39101. However cases with a more evident and numerous bursts are obtained during the H-mode biasing induced phase. In this section a deeper analysis on the edge features of the phenomena associated to these bursts is provided. An example of edge monitoring during a bursty phase in a SN shaped shot, is shown in Figure 12. The picture shows, on the left, the time behavior of the I_{sat}, taken as a proxy of local plasma density, measurements obtained at different distances from the LCFS, $\Delta r_{LCFS} = r - r_{LCFS}$ so that $\Delta r_{LCFS} > 0$ indicates a measurement outside the LCFS, the color code used for the signals is shown by the vertical lines on right panels radial profiles. As for reference of the burst occurrence, the D_α signal is shown with a continuous black line which evidences the presence of four major peaks in the selected time window. Ranging from the deeper inserted measurement at $\Delta r_{LCFS} \sim -0.02m$ to the outer one at $\Delta r_{LCFS} \sim 0.04m$ a strong modification of the signal at the burst occurrence is observed in the whole explored range. A clear drop is observed in the signal I_{sat} level for $\Delta r_{LCFS} < 0$, while large bursts emerge from background at the outer measurement points, at $\Delta r_{LCFS} > 0$. To better analyze this behavior, the average profiles of I_{sat} and of its root-mean-square $rms(I_{sat})$ are shown in the two panels on the right. In particular as an example a phase during the occurrence of one of the bursts and the phase preceding this event are compared. These two phases are delimited by red and black dashed lines respectively and the same color code is used in the profiles. A strong I_{sat} gradient, related to the H-mode establishment, is observed in the inter-event phase (black symbols), while a flattening of the profile is observed during the burst itself. In particular a drop of the signal is observed in the inner region, while a relative increase is transiently observed in the SOL, $\Delta r_{LCFS} > 0$. The $rms(I_{sat})$ radial profile shows a general increase along the whole explored region, indicating a turbulence increase in this phase. In addition it exhibits, in the event phase, a very strong increase in the SOL region with respect to the inter-event phase, with a peak around $\Delta r_{LCFS} = 0.15m$. These data are consistent with the indication of transient outer ejection of plasma density, corresponding to the D_α bursts. The Figure 13 provides the analogous analysis but for the floating potential signals. In this case a larger number of radially distributed measurements are available so that a more detailed average profile can be provided. Strong modifications of the

whole V_f signals is observed to correspond to the D_α bursts (black continuous line), indicating a reduction of the average radial electric field during events. The average V_f radial profiles example shown on the right panel confirms this picture: a strong flattening of $V_f(r)$ is observed at the event phase, without however reaching the level of the L-mode phase characterizing the profile before the biasing operation. The level of V_f fluctuations, as represented by the rms, is also in this case generally increasing in the explored region.

Further information on the edge bursts detailed features are provided in Figure 14. D_α is compared with the $I_{sat}(r,t)$ measured in the SOL at $r - r_{LCFS}$ 1 cm, in a time window including the one of Figure 12. A clear correlation with D_α of $I_{sat}(r,t)$ bursty behavior, involving the whole measured profile, is observed. Figure 14 shows also two inserts with increased magnification details of the same event found in the time window from 839 ms to 841 ms. In this case a multiple fragmented density structure is observed. In the maximum zoom insert in Figure 14 the detail on few of these fragments exhibits a behavior consistent with their radial propagation. A radial velocity propagation of such fragments is estimated of the order of 10 m/s, corresponding to $\sim 0.001 \cdot c_s$, where $c_s \sim 10^4 m/s$ is the local ion sound velocity.

The Figure 15 provides further details on these events coming from the parallel vorticity, ω_t, and fluctuations of the parallel current density, J_t, associated to the D_α peaks. Their respective time behavior and spectrograms are shown in the same time window and same shot of Figure 14.

A first observation in Figure 15 deserves the vorticity spectrogram, $S\omega_t(t)$, behavior. The occurrence of D_α bursts, shown in Figure 14, is clearly correlated with the abrupt and wide spreading to all the frequencies events observed on the $S\omega_t(t)$. This spectrogram behavior indicates the presence of localized structures crossing the probe location. In addition the $\omega_t(t)$ exhibits simultaneously strong negative peaks indicating that these structures are vortices, rotating in the cross-field plane. It is interesting to note that similar feature was observed in the turbulent filaments in the edge region of all magnetic configuration fusion devices as well as in linear devices [24, 25]. D_α correlated bursty spreading is also observed in the δJ_t spectrogram, $S\delta J_t(t)$, (Figure 15 top panels), corresponding to the bipolar peaks observed in the $\delta J_t(t)$ time evolution, left panel. These observations confirm also the electromagnetic (EM) features of the observed structures as expected for ELMs [26, 27]. In particular these events are current filaments and the present diagnostic setup allows a direct current density measure, which in this case is of the order of $0.5 kA/m^2$. Similar features are found in the ELM structure EM characterization in the COMPASS experiment [28], where the same diagnostic concept was applied [29], supporting the hypothesis that the observed events can be interpreted as ELMs.

Regarding the limited circular shape, an analogous analysis was performed on the edge EM structures associated to the D_α peaks. As an example, the D_α events observed during the biasing induced H-mode phase in the shot ♯39101 (see Figure 11) are evaluated, the results are shown in Figure 16. The detected current density peaks (top-left panel) are less apparent with respect to the Figure 15 case and this feature affects the corresponding $S\delta J_t(t)$ spectrogram broadening. Nevertheless also sudden spreading of the spectrum are still visible corresponding to the D_α events. Strong bursts on the parallel vorticity are found also in this case, but with a different shape, dipolar instead of monopolar peaks.

The mechanism of vorticity selection due to the local flow shearing rate and sign is well assessed in fluid dynamics. It was also experimentally identified in the RFP

and stellarator fusion devices [30, 25] furthermore, from the theoretical point of view, this mechanism was invoked as the basis of non-diffusive transport in gyrokinetic simulations [31].

On this regard it is worth to note that $\delta\omega_t$ dipolar peaks shown in Figure 16 are detected on top of an average local vorticity (or shearing rate), much lower than to one of Figure 15. The observed $\delta\omega_t$ peak shape difference could be due to the different local velocity shear characterizing the two examined cases. A more weakly effect in the vorticity selection in the latter one could be expected, were dipolar vorticity structures are found.

4.2. H-mode quasi-coherent modes investigation

As shown in Figure 11 spectrograms, the biasing induced H-mode regime is characterized also by the presence of coherent modes in the magnetic fluctuations. In the circular limited shape, coherent modes are observed also on electrostatic fluctuations. It is worth mentioning that the presence of magnetic modes during ohmic or NBI assisted H-mode regimes, was recently documented in tokamaks, i.e. in DIII-D [32] and COMPASS [33], in particular during the ELM-free or in the inter-ELM phase.
To gain insight on the present experimental results the RFX-mod ISIS system was exploited [34], which also revealed the modes under study. The ISIS system includes in-vacuum pick-up coils measuring the three components of the fluctuating magnetic field magnetic sensors located on the vessel wall and arranged in poloidal and toroidal arrays, so to allow spatial characterization of magnetic modes.

In Figure 17 the coherence between pairs of magnetic signals provided by closest neighborhood sensors and measuring the poloidal component time derivative $\dot{B}_\theta$ are shown, as a function of time and frequency. In particular, the coherence between sensors located at the HFS (top panels) is compared with that provided by the coils at the LFS (bottom panels), for the two reference discharges,♯39101 (circular) and ♯39135 (SN). Coherent modes are observed in all the analyzed cases with similar time behavior comparing LFS and HFS. It can be observed however that, different frequencies characterize the modes in the LFS with respect to the ones at HFS respectively and this feature is particularly apparent in the SN case.
The black continuous line represents the time evolution of an Alfvénic frequency, being proportional to $f_A \sim B/n_e^{1/2}$, where B is the main magnetic field and n_e the electron density. A rather similar behavior can be recognized comparing the modes frequency and f_A time evolutions. It is worth considering that f_A is an average estimate and does not take into account the radial modulation of the parameters involved.
In Figure 18, the toroidal mode numbers characterizing the modes for the two reference discharges are estimated. The measurement is provided by the so called two-point technique between two pick-up coils directly faced to the plasma and pertaining to the GPI system [35]. The minimum toroidal distance of $\Delta\phi = 22mm$ allows in this case to measure very high toroidal mode numbers ($n_{max} = \frac{\pi}{\Delta\phi} \approx \pm 143$). Also in this case the analysis is based on the time derivative of the poloidal component of the magnetic fluctuating field. Different values of toroidal mode number, n, in the range $n \sim 10 - 20$ are estimated for modes at different frequencies.
As a first draft conclusion these observations exhibit similar features to those described by Melnikov et al. [33] regarding modes of Alfvénic nature: in both cases the modes occur only during the H-mode phase, are not symmetric with respect to the High and

Low Field Sides and present an Alfvénic behavior of the frequency. The value of the toroidal mode numbers instead is quite different. Anyway, more analysis are required to better characterize these modes and identify their nature.

5. Discussion and conclusions

Regimes with improved confinement were obtained in RFX-mod experiment operated as tokamak. The most reproducible H-mode conditions were obtained via edge biasing, with a negative bias with respect to the first wall. This operation corresponds to the enhancement of the naturally occurring poloidal $E \times B$ shear layer revealed during the, L-mode. An abrupt increase of the edge radial gradient of plasma electron pressure and poloidal flow $v_{E \times B}$ were obtained in the surrounding of the LCFS, in both circular and SN shaped discharges. Within the incertitude of the separatix radial position, the characteristic pressure length is lower in the circular case and the point of null V_f is outer in the SN case. In both configurations, modes in the 70-100kHz range are observed in the magnetic spectrogram. On the other side only in the circular configuration a simultaneous presence of similar modes are detected in the electrostatic signals. A further indication supporting of the H-mode nature of the obtained regime is provided by the magnetic modes characterizing the improved confinement phase, which exhibit noticeable similarities with the ones observed in NBI induced H-mode regimes tokamak devices. In some cases, in both configurations, the presence of ELM-like structures are detected in the D_{alpha} signals. Those structures are found to be filamentary fragmented structures, with density features consistent with their radial propagation. Furthermore they appear as vortices rotating in the cross-field plane and exhibit EM features. It is worth noting that their associated local current density and vorticity fluctuations, parallel to the average magnetic field, were measured simultaneously for the first time. The analysis of time evolution of edge radial profiles allowed the reconstruction of a sequence consistent with the the cyclically establishment of strong edge gradients followed by the expulsion of cluster of filamentary fragments (ELMs)with electromagnetic features. In conclusion the obtained operating scenario can be considered relevant and open to the future possibility to exploit the state of art of magnetic boundary control available in RFX-mod in the next step operation phase [17] of the upgraded device.

Acknowledgments

References

[1] Piovesan P, Bonfiglio D, Auriemma F, Bonomo F, Carraro L, Cavazzana R, De Masi G, Fassina A, Franz P, Gobbin M *et al.* 2013 *Physics of Plasmas (1994-present)* **20** 056112
[2] Zanca P, Marrelli L, Paccagnella R, Soppelsa A, Baruzzo M, Bolzonella T, Marchiori G, Martin P and Piovesan P 2012 *Plasma Physics and Controlled Fusion* **54** 094004
[3] Spolaore M, Agostini M, Momo B, Rea C, Vianello N, Zuin M, Cavazzana R, De Masi G, Innocente P, Marrelli L *et al.* 2015 *Nuclear Fusion* **55** 063041

[4] Vianello N, Rea C, Agostini M, Cavazzana R, Ciaccio G, De Masi G, Martines E, Mazzi A, Momo B, Spizzo G *et al.* 2014 *Plasma Physics and Controlled Fusion* **57** 014027

[5] Piron C e a 2015 Real-time simulation of internal profiles in the presence of sawteeth using the raptor code and applications to asdex upgrade and rfx-mod *42nd EPS Conference on Plasma Physics* (*Europhysics Conference Abstacts* vol 39E) (Lisbon, Portugal: EPS) p P1.145

[6] Gobbin M e a 2015 Runaway electron mitigation by resonant and non-resonant magnetic perturbations in rfx-mod tokamak discharges *42nd EPS Conference on Plasma Physics* (*Europhysics Conference Abstacts* vol 39E) (Lisbon, Portugal: EPS) p O4.136

[7] Kirk A, Chapman I, Harrison J, Liu Y, Nardon E, Saarelma S, Scannell R, Thornton A *et al.* 2012 *Plasma Physics and Controlled Fusion* **55** 015006

[8] Van Oost G, Adamek J, Antoni V, Balan P, Boedo J, Devynck P, Ďuran I, Eliseev L, Gunn J, Hron M *et al.* 2003 *Plasma physics and controlled fusion* **45** 621

[9] Dhyani P, Ghosh J, Chattopadhyay P, Tanna R, Raju D, Joisa S, Chattopadhyay A K, Basu D, Ramaiya N, Kumar S *et al.* 2014 *Nuclear Fusion* **54** 083023

[10] Liu H, Hu Q, Chen Z, Yu Q, Zhu L, Cheng Z, Zhuang G and Chen Z 2017 *Nuclear Fusion* **57** 016003

[11] Cavazzana R et a Real time control of electron density on rfx-mod tokamak discharges; ieee transactions on nuclear science, submitted

[12] Marchiori G, Finotti C, Kudlacek O, Villone F, Zanca P, Abate D, Cavazzana R, Jackson G, Luce T and Marrelli L 2016 *Fusion Engineering and Design* **108** 81–91

[13] Kudlacek O, Zanca P, Finotti C, Marchiori G, Cavazzana R and Marrelli L 2015 *Physics of Plasmas* **22** 102503

[14] FLIR A655sc infrared camera http://www.flir.com/science/display/?id=46802

[15] Maschio A, Piovan R, Benfatto I, Collarin P, De Lorenzi A, Fellin L, Gaio E, Gray J, Hood M and Toigo V 1995 *Fusion Engineering and Design* **25** 401–424

[16] Carraro L e a 2016 Tokamak experiments in rfx-mod with polarized insertable electrode *43rd EPS Conference on Plasma Physics* (*Europhysics Conference Abstacts* vol 40A) (Leuven, Belgium: EPS) p P5.014

[17] Zuin M et a Overview of the rfx-mod fusion science activity; nuclear fusion, submitted

[18] Spolaore M, Vianello N, Agostini M, Cavazzana R, Martines E, Serianni G, Scarin P, Spada E, Zuin M and Antoni V 2009 *Journal of Nuclear Materials* **390** 448–451

[19] Martin P, Murari A, Buffa A, Marrelli L, Baker W, Gadani G, Hemming O, Manduchi G, Parini A, Taliercio C *et al.* 1997 *Review of scientific instruments* **68** 1256–1260

[20] Franz P, Marrelli L, Murari A, Spizzo G and Martin P 2001 *Nuclear fusion* **41** 695

[21] Kudlacek O e a 2015 H-mode accessibility in ohmic discharges on rfx-mod *42nd EPS Conference on Plasma Physics* (*Europhysics Conference Abstacts* vol 39E) (Lisbon, Portugal: EPS) p P4.154

[22] Liang Y 2015 Edge localized mode (elm) *Active Control of Magneto-hydrodynamic Instabilities in Hot Plasmas* (Springer) pp 143–181

[23] Leonard A 2014 *Physics of Plasmas* **21** 090501

[24] D Ippolito D, Myra J and Zweben S 2011 *Physics of Plasmas* **18** 060501

[25] Spolaore M, Vianello N, Furno I, Carralero D, Agostini M, Alonso J, Avino F, Cavazzana R, De Masi G, Fasoli A *et al.* 2015 *Physics of Plasmas* **22** 012310

[26] Kirk A, Ayed N B, Counsell G, Dudson B, Eich T, Herrmann A, Koch B, Martin R, Meakins A, Saarelma S *et al.* 2006 *Plasma physics and controlled fusion* **48** B433

[27] Vianello N, Naulin V, Schrittwieser R, Müller H, Zuin M, Ionita C, Rasmussen J, Mehlmann F, Rohde V *et al.* 2011 *Physical review letters* **106** 125002

[28] Spolaore M, Kovařík K, Stöckel J, Adamek J, Dejarnac R, Ďuran I, Komm M, Markovic T, Martines E, Panek R *et al.* 2016 *Nuclear Materials and Energy*

[29] Kovarik K, Duran I, Stockel J, Seidl J, Adamek J, Spolaore M, Vianello N, Hacek P, Hron M and Panek R 2017 *Review of Scientific Instruments* **88** 035106

[30] Spolaore M, Antoni V, Spada E, Bergsåker H, Cavazzana R, Drake J R, Martines E, Regnoli G, Serianni G and Vianello N 2004 *Physical review letters* **93** 215003

[31] Sanchez R, Newman D E, Leboeuf J N and Decyk V 2011 *Plasma Physics and Controlled Fusion* **53** 074018

[32] Diallo A, Hughes J, Greenwald M, LaBombard B, Davis E, Baek S, Theiler C, Snyder P, Canik J, Walk J *et al.* 2014 *Physical review letters* **112** 115001

[33] Melnikov A, Markovic T, Eliseev L, Adámek J, Aftanas M, Bilkova P, Boehm P, Gryaznevich M, Imrisek M, Lysenko S *et al.* 2015 *Plasma Physics and Controlled Fusion* **57** 065006

[34] Serianni G, Bolzonella T, Cavazzana R, Marchiori G, Pomaro N, Lotto L, Monari M and Taliercio C 2004 *Review of scientific instruments* **75** 4338–4340

[35] Agostini M, Scarin P, Spizzo G, Vianello N and Carraro L 2014 *Plasma Physics and Controlled Fusion* **56** 095016
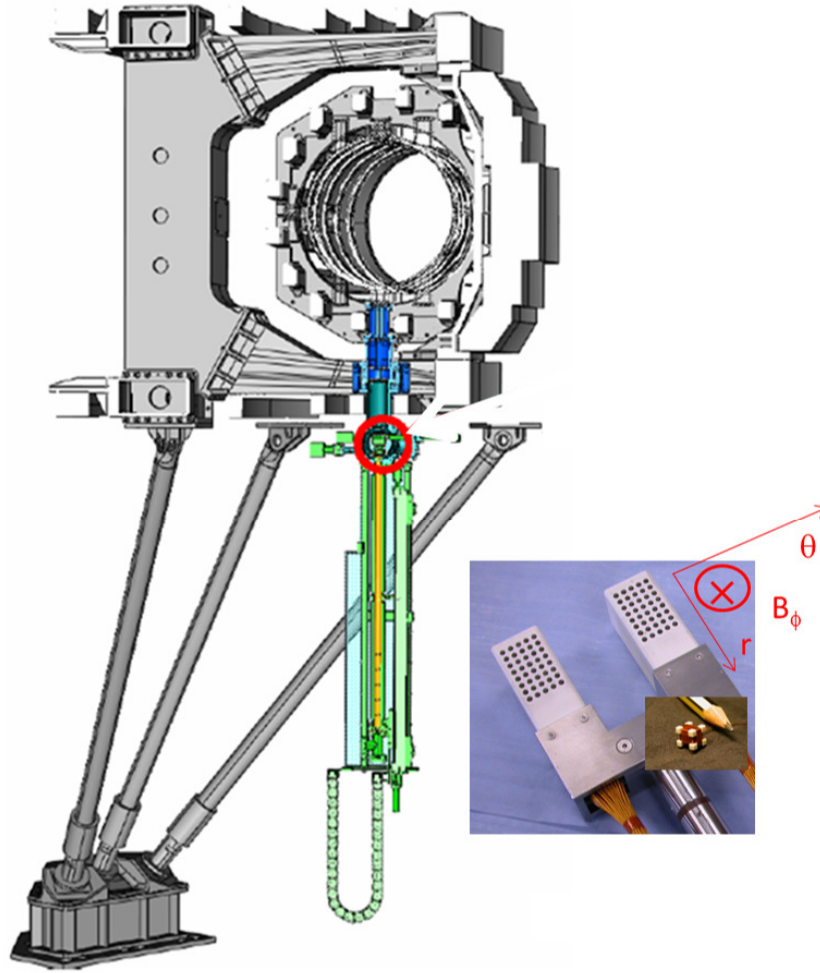
Figure 1: RFX-mod section at the toroidal position of the biasing electrode insertable system (mechanical parts in colors). In the square picture the U-probe insertable probe head is shown with indication of the used reference frame.
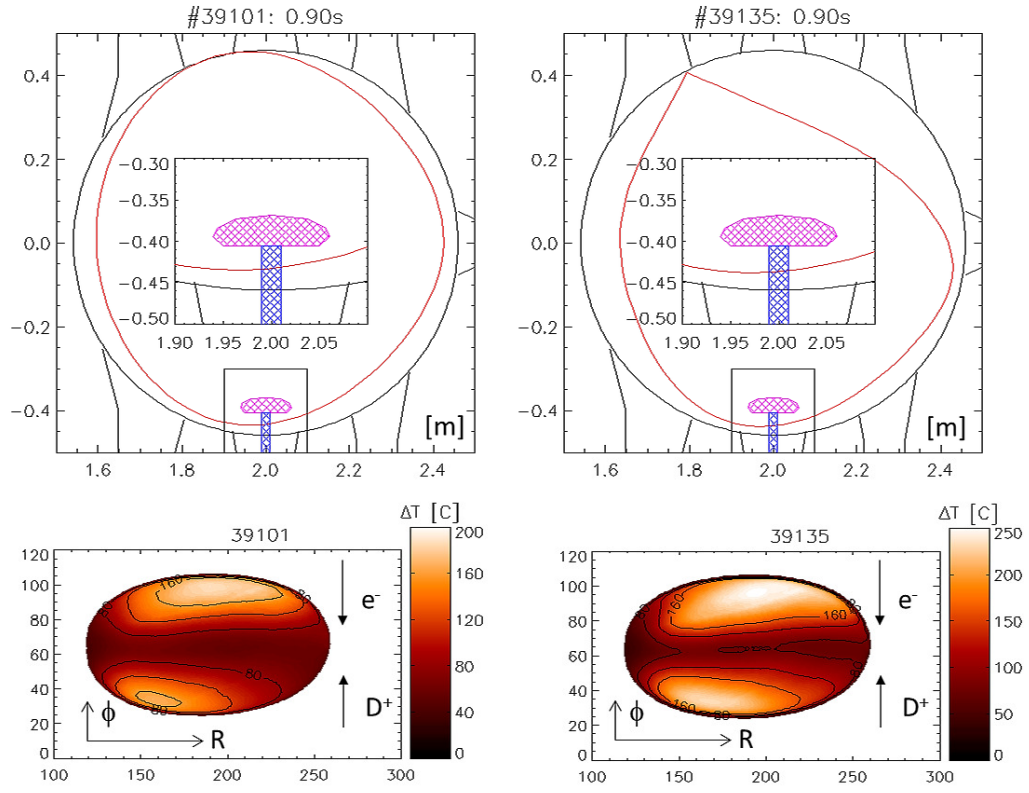
Figure 2: Poloidal section of the vacuum chamber with the reconstruction of the LCFS position, red line, and the corresponding electrode head (magenta) insertion. The two top panels refer to H-mode phase obtained for the circular shape (shot ♯39101) and SN shape (shot ♯39135). Bottom panels: Thermographic image of the biasing electrode side exposed to plasma, for the same shots.
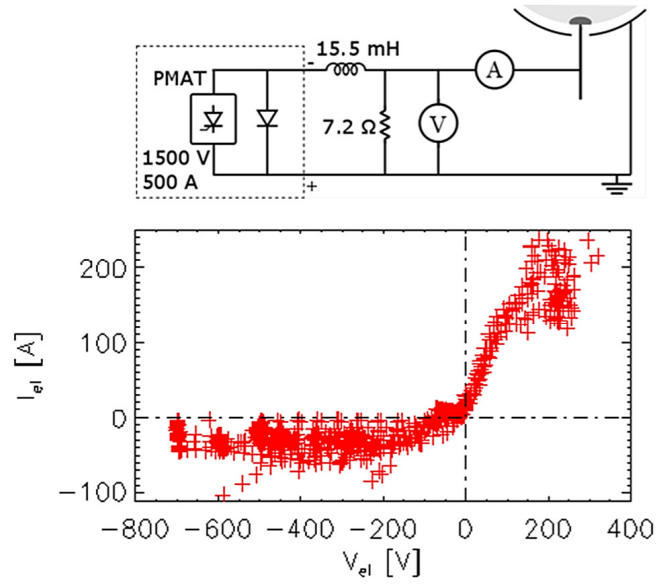
Figure 3: Electrical scheme used for the biasing (top). Electrode voltage V_{el} and corresponding electrode current I_{el} explored during the biasing experimental campaign.
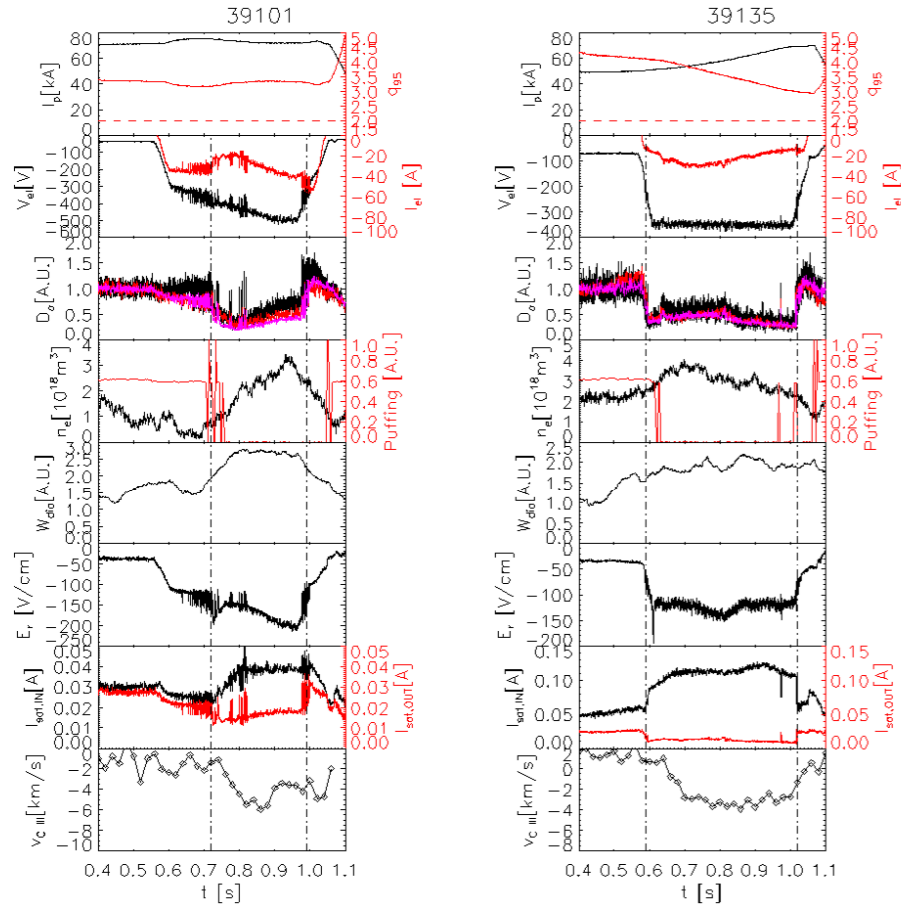
Figure 4: Time evolution of the applied V_{el} and I_{el}, of the main discharge parameters, and of some representative edge quantities. Circular shape ♯39101 (left) SN shape ♯39135 (right).
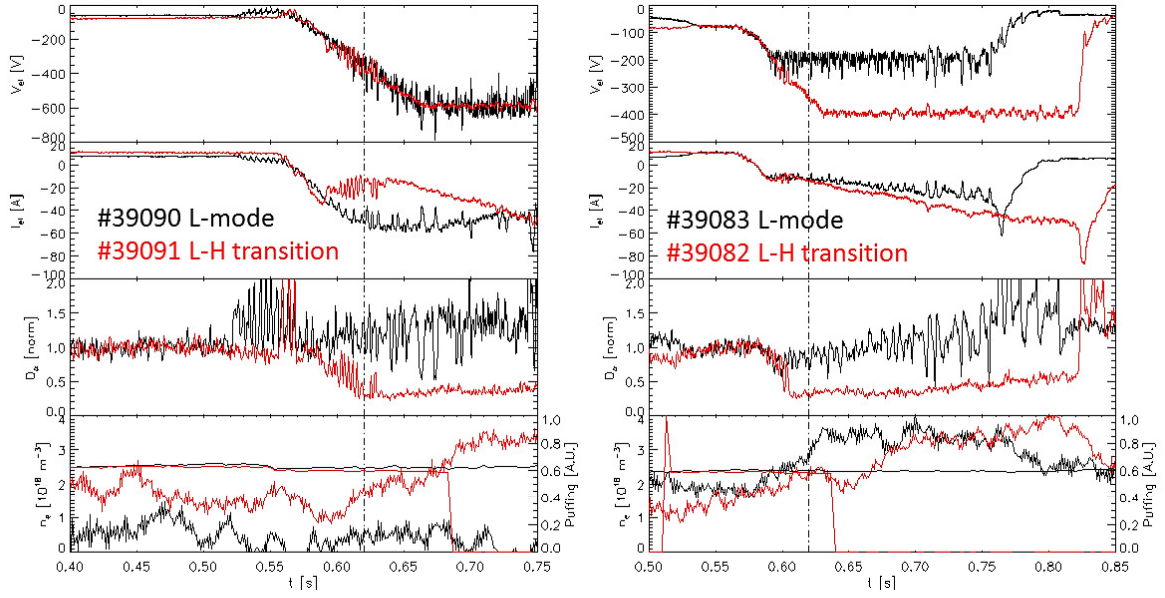
Figure 5: Examples of obtained transition related to plasma density level (right panel) or to applied electrode voltage V_{el}.
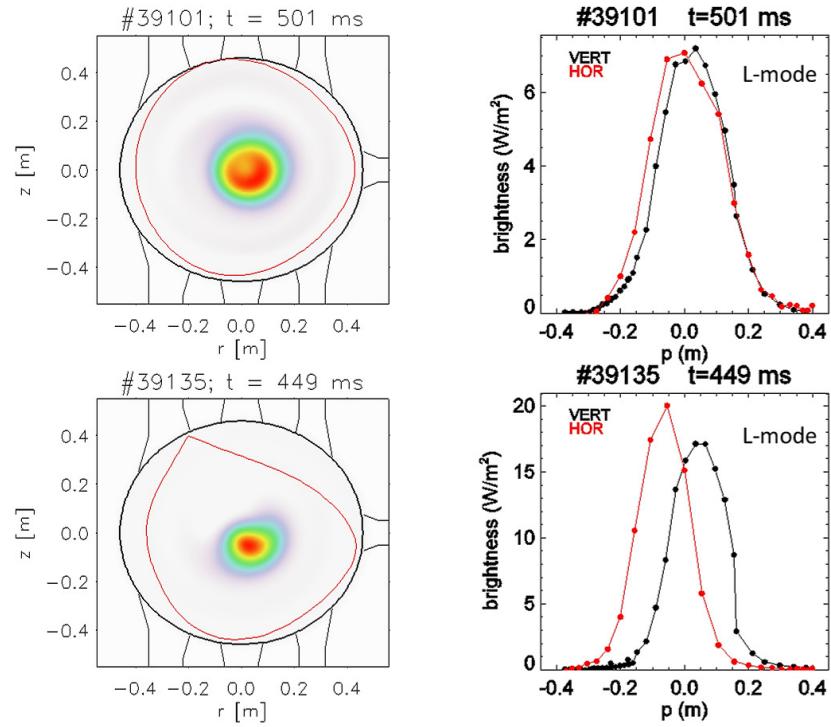
Figure 6: Tomographic reconstruction of the SXR emissivity in the poloidal section ($\phi =$) (left column). Corresponding brightness (line integral) as provided by horizontal and vertical profiles data-set (right column). Data obtained in the phase preceding electrode biasing, for shots ♯39101 (circular) and ♯39135 (SN) respectively.
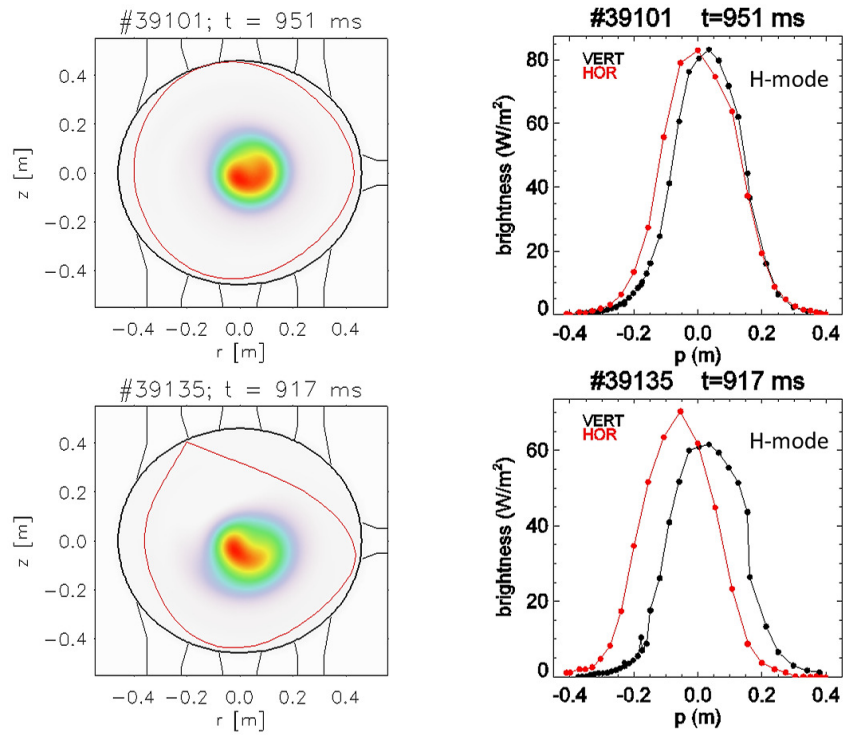
Figure 7: Same as in Figure 6, with measurements obtained during the H-mode phase for shots ♯39101 (circular) and ♯39135 (SN) respectively.
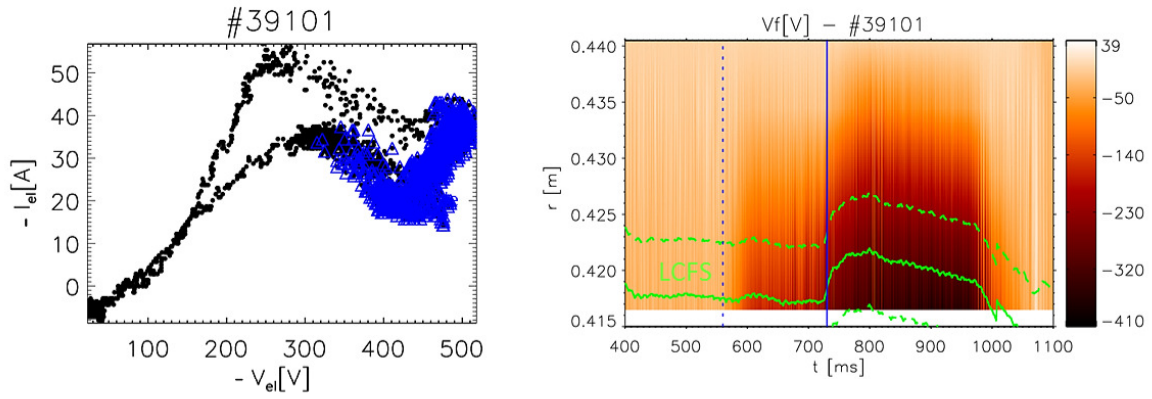
Figure 8: Left: Electrode Voltage-Current characteristic during shot ♯39101, H-mode phase highlighted (blue triangles). Right: time evolution of $V_f(r,t)$ measured by one U-probe tower, local r_{LCFS} (green continuous line) and $r_{LCFS} \pm 5mm$ (green dashed lines).
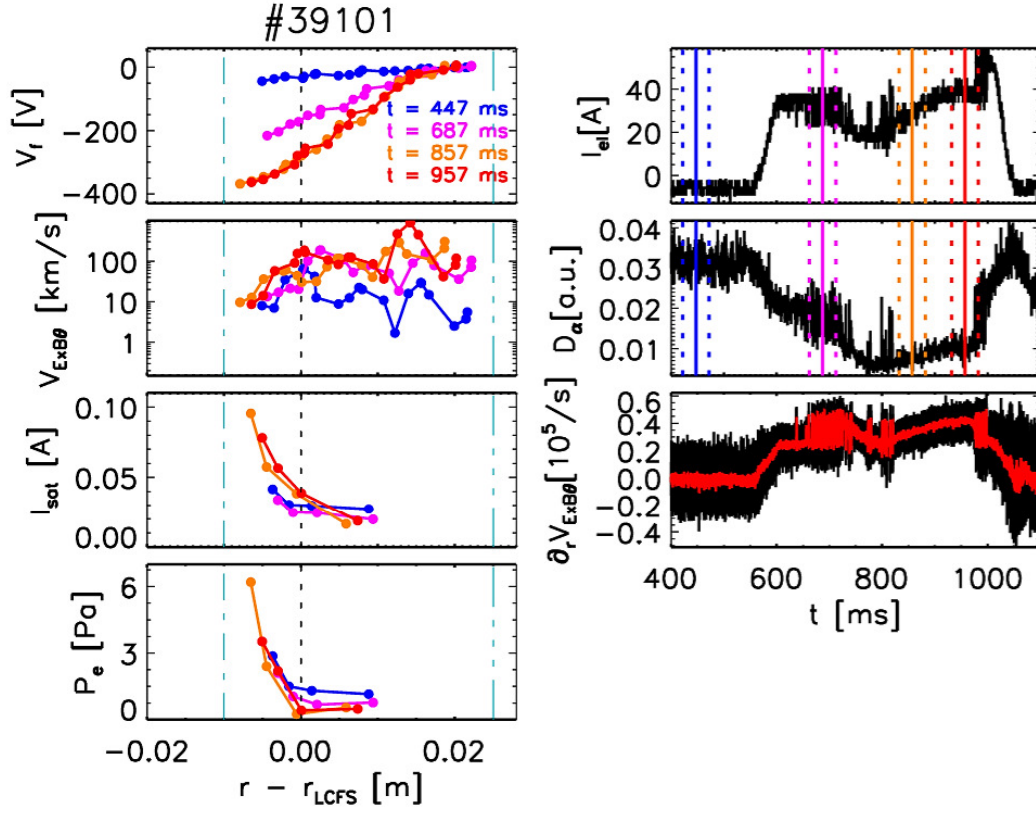
Figure 9: Average radial profiles of V_f, poloidal $v_{E \times B}$, I_{sat}, P_e as a function of relative radial distance from the LCFS, measured at different times t over $t \pm 25$ ms time window (left); time evolution of I_{el}, D_α and edge $dv_{E \times B}/dr$ measured at $r = 0.422m$ during electrode operation (right); data from circular shaped shot $\sharp39101$ (circular). Vertical dashed turquoise lines are provided for a easier comparison with Figure 10.
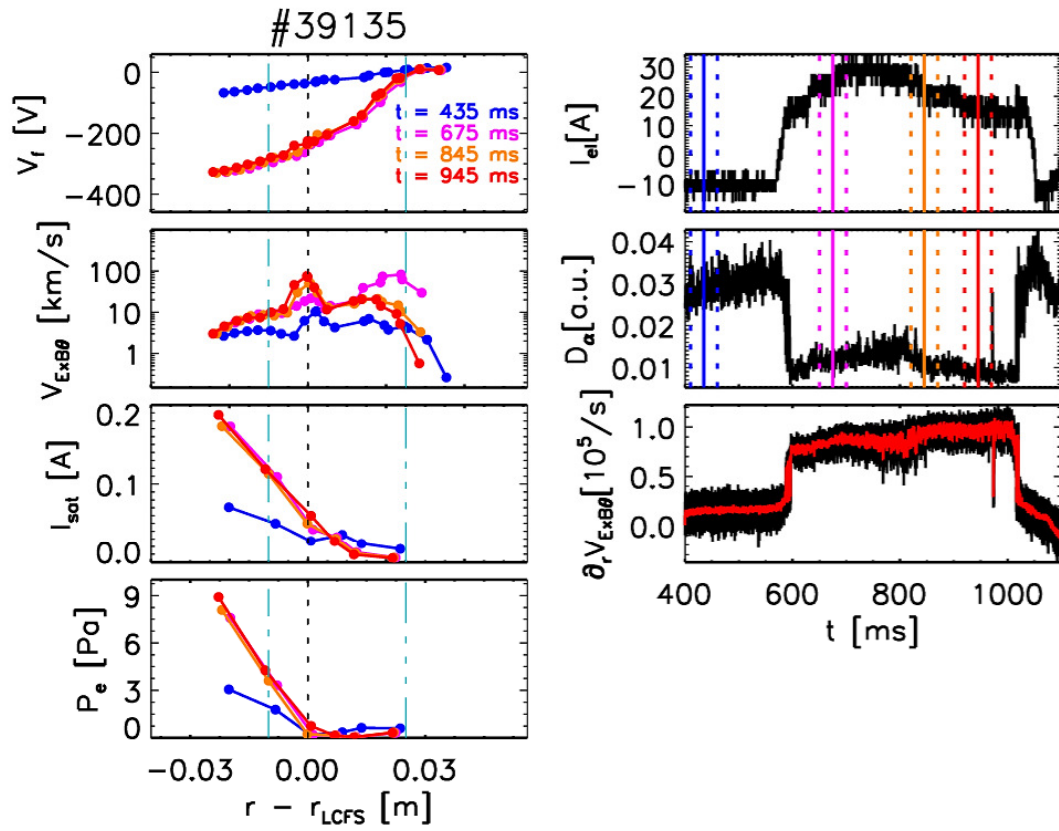
Figure 10: Same as in Figure 9 with data from SN shaped shot ♯39135 (SN). Vertical dashed turquoise lines are provided for a easier comparison with Figure 9.
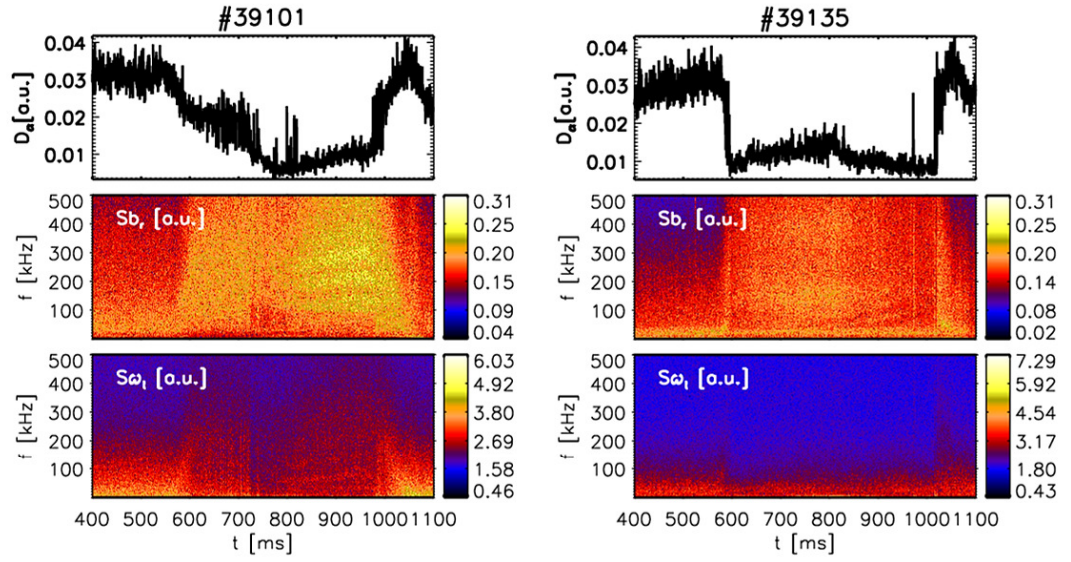
Figure 11: Time evolution of D_α during electrode operation compared with spectrogram of δb_r and ω_t, data from shots $\sharp$39101 (circular) and $\sharp$39135 (SN).
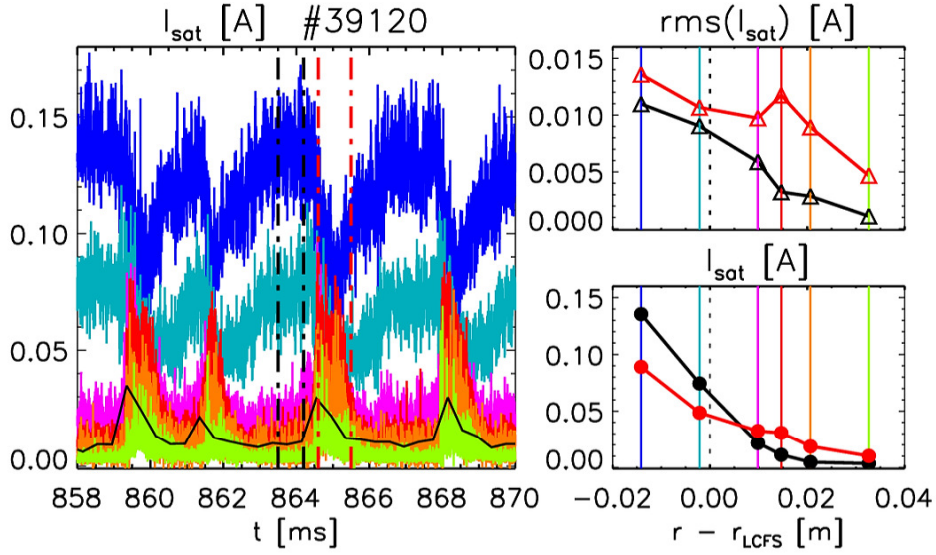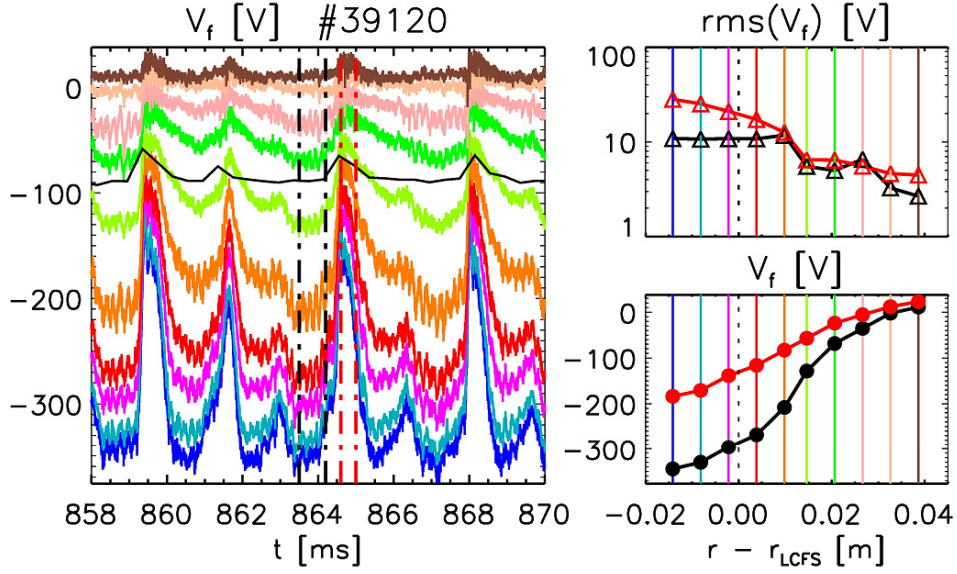
Figure 12: Left panel: I_{sat} measured at different distances $r - r_{LCFS}$, during a ELMy phase detected on D_α signal, shown in black continuous line [a.u.]). Color code position follows the vertical lines in the right panels. Right panels:average radial profiles of I_{sat} and of its rms, as a function of $r - r_{LCFS}$, estimated during the inter-ELM (black) and during ELM burst (red) phases as indicate respectively by the vertical dashed lines in the left panel.

Figure 13: Left panel: V_f measured at different distances $r - r_{LCFS}$, during a ELMy phase detected on D_α signal, shown in black continuous line [a.u.]). Color code position follows the vertical lines in the right panels. Right panels:average radial profiles of V_f and of its rms, as a function of $r - r_{LCFS}$, estimated during the inter-ELM (black) and during ELM burst (red) phases as indicate respectively by the vertical dashed lines in the left panel.
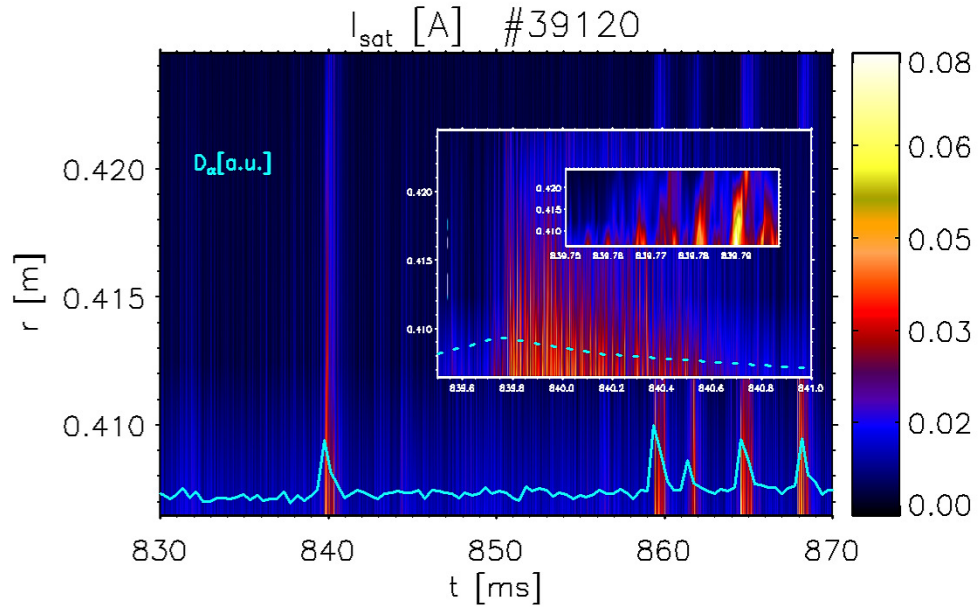
Figure 14: Time evolution of the $I_{sat}(r)$ radial profile, at $r - r_{LCFS} \geq 1$ cm, during H-mode in presence of ELM-like events. The corresponding $D_\alpha(t)$ is over-plotted for comparison; data from SN shot ♯39120.
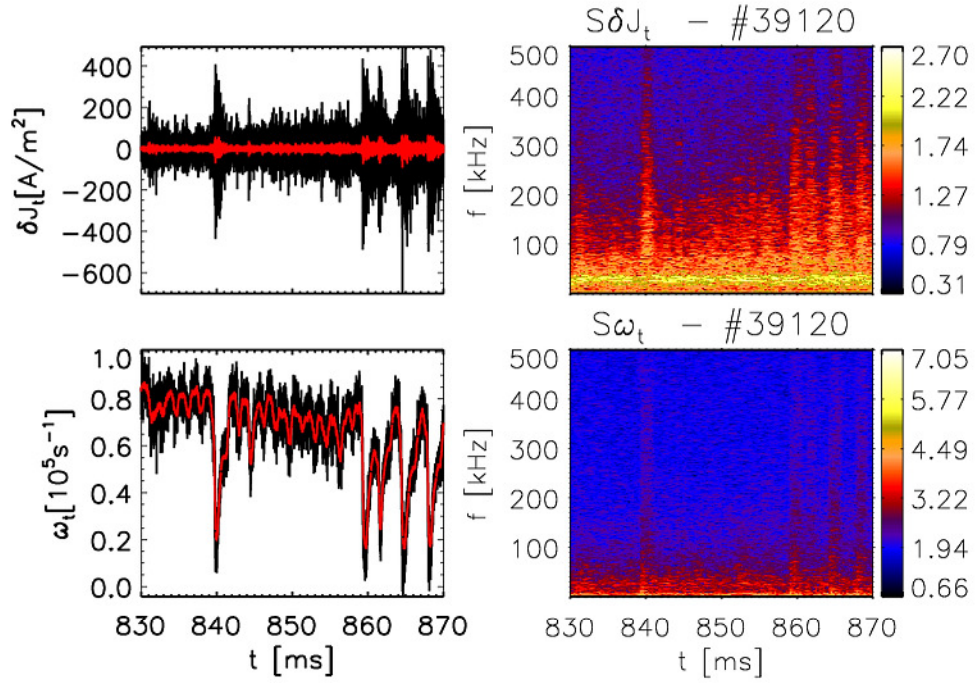
Figure 15: Time behavior of ω_t, and δJ_t fluctuations, smoothed signal in (red); their respective spectrograms are shown on the left. Data obtained during the H-mode phase with ELMs-like events on SN shaped shot $\sharp$39120.
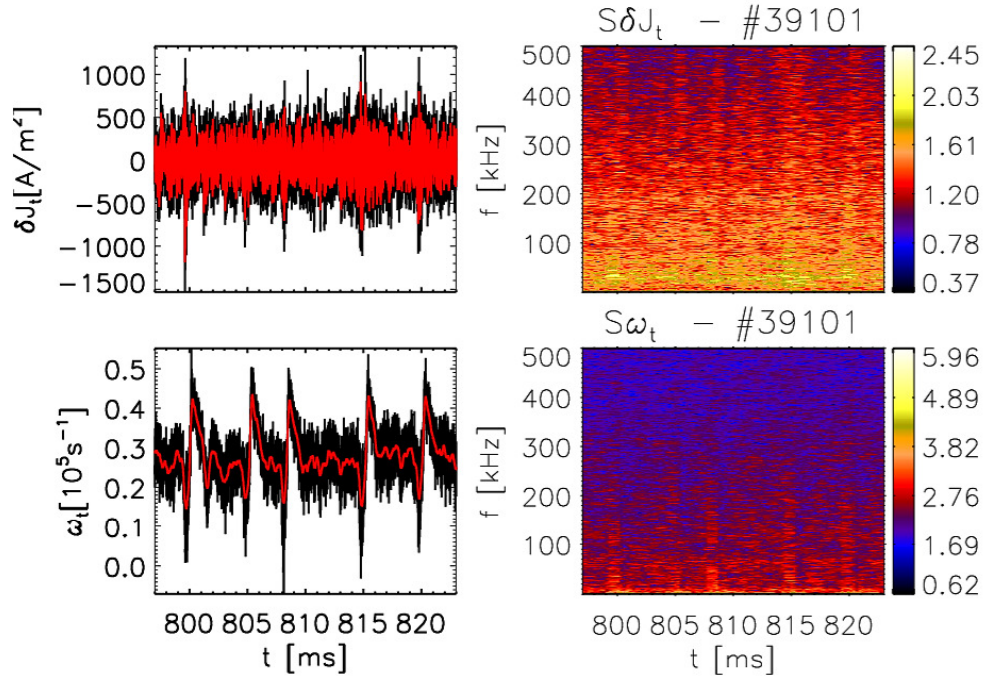
Figure 16: Time behavior of ω_t, and δJ_t fluctuations, smoothed signal in (red); their respective spectrograms are shown on the left. Data obtained during the H-mode phase with ELMs-like events on circular shaped shot $\sharp 39101$.
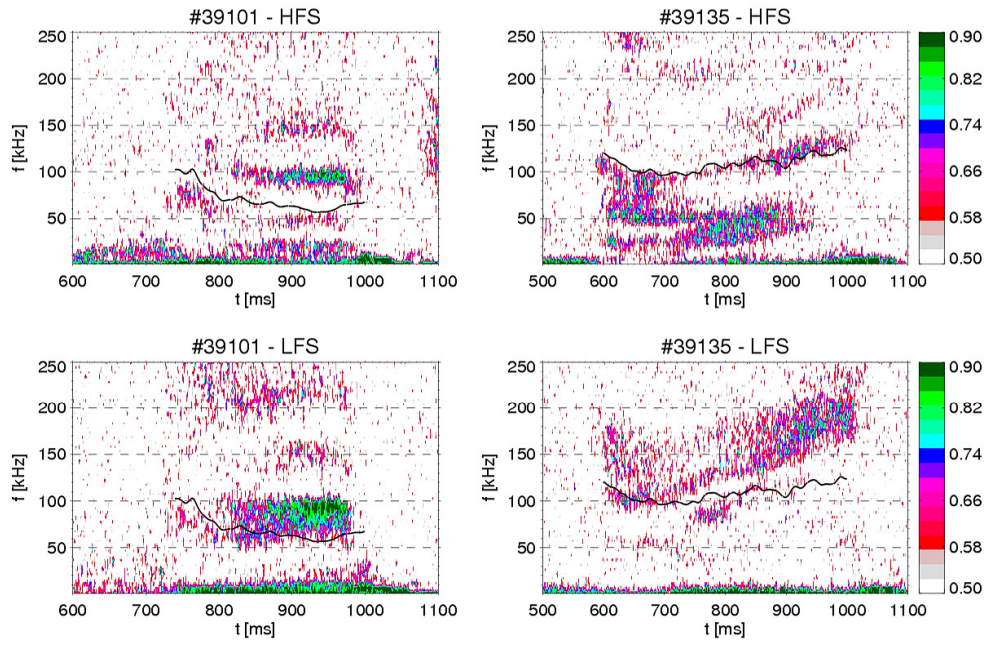
Figure 17: Spectrogram of the coherence between couple of closest neighborhood magnetic sensors from the ISIS system, measuring the $\dot{B}_\theta$ component respectively on LFS and HFS, for the shots ♯39101 (circular) and ♯39135 (SN). The black continuous line represents the time evolution of the Alfvénic frequency.
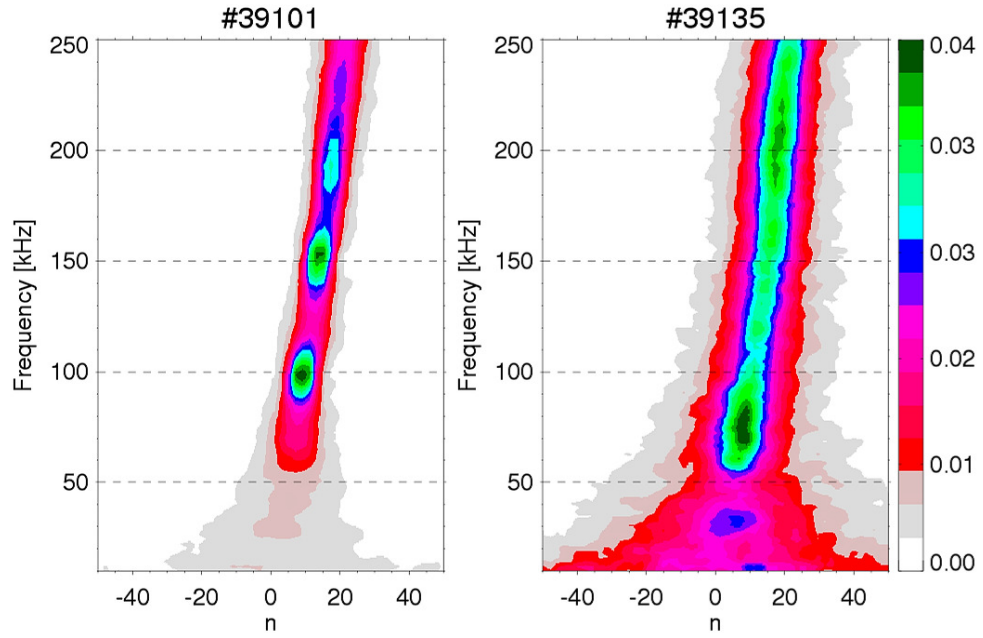
Figure 18: Toroidal mode number estimate for the different frequency modes observed in Figure 17; data from shots ♯39101 (circular) and ♯39135 (SN).